Detection of Silver Nanoparticles by Optical Planar Waveguide Based Lossy Mode Resonance Sensor Platform

Yu-Cheng Lin*

Department of Electronic Engineering, Ming Chuan University

ABSTRACT

Silver nanoparticles (AgNPs) are a crucial type of nanomaterial with vast potential applications in the fields of biomedical research and materials science. However, most detection instruments are unable to monitor the real-time generation rate or duration of AgNPs during the synthesis process. This paper demonstrates the use of an optical planar waveguide-based lossy mode resonance (OPWLMR) sensor to build a sensing platform combined with a photo-assisted reduction method for the in-situ generation of AgNPs and to simultaneously observe the lossy mode resonance (LMR) wavelength shift. The OPWLMR sensor exhibits a high sensitivity of 1008.9 nm/RIU. Experimental results reveal that a minimum driving voltage of approximately 19 V (under an illumination intensity of 41.1 W/m²) and the required duration for AgNPs deposition on the sensor is about from 15 to 20 minutes. The size distribution of AgNPs showed bimodal distribution with mean sizes of 2.2 nm and 41.8 nm, respectively.

Keywords: silver nanoparticles, photo-assisted reduction, LED array

以光學平面波導損耗模態共振感測器平台偵測銀奈米粒子

林鈺城*

銘傳大學電子工程學系

摘 要

銀納米粒子(AgNPs)是一種重要的納米材料,在生物醫學研究和材料科學具有廣泛的潛在應用。然而,大多數檢測儀器無法即時監測 AgNPs 的生成速率或時間。本文展示了基於損耗模式共振光學平面波導(OPWLMR)感測器,構建 AgNPs 感測平台的方法。結合光輔助還原法來生成 AgNPs,同時觀察損耗模式共振(LMR)波長的變化。結果顯示,OPWLMR 感測器的靈敏度達到 1008.9 nm/RIU。根據實驗,生成 AgNPs 所需的最小光輔助驅動電壓約為 19 V(照度為 41.1 W/m²),而 AgNPs 在感測器上沉積所需的時間約為 15 至 20 分鐘。AgNPs 的大小分布呈雙峰分布,平均大小分別為 2.2 nm 和 41.8 nm。

關鍵詞:銀奈米粒子,光輔助還原,LED陣列

文稿收件日期 110.10.19; 文稿修正後接受日期 111.1.24; *通訊作者 Manuscript received October. 19, 2021; revised Jan. 24, 2022; * Corresponding author

I. INTRODUCTION

Silver nanoparticles (AgNPs) have garnered significant attention due to their unique properties and potential applications in various fields. With diameters ranging from 1 to 100 nm, AgNPs have been investigated for their use as biosensors, antibacterial agents, cell imaging agents, drug delivery vehicles, and wound healing agents in biomedical research [1]. They also have promising applications in Surface-Enhanced Raman Scattering (SERS) for detecting biological molecules [2]. In electronics, AgNPs have been demonstrated as highly efficient conductive materials and conductive pads for flexible electronics [3]. In optics, AgNPs can serve as optical filters, enhancers, and surface plasmon resonance (SPR) sensors to improve sensitivity and detection limits [4]. In material science, AgNPs can function as catalysts and electrochemical energy storage materials, improving reaction efficiency and rate. As such, AgNPs are an important nanomaterial with vast potential applications, and further research is necessary to optimize their properties for these applications.

There are various methods available for producing AgNPs, including chemical reduction, electrochemical synthesis, photochemical synthesis, green synthesis, and photo-assisted reduction method. The choice of production method is dependent on the desired properties of the nanoparticles and the specific application [5]. Chemical reduction is a simple and cost-effective method, but may result in a broad size distribution of particles [6]. Electrochemical synthesis can produce nanoparticles with a narrower size distribution, but it requires specialized equipment. Photochemical synthesis produce nanoparticles with controlled size and shape, but may require expensive equipment. Green synthesis employs natural reducing agents and is environmentally friendly, but the size distribution may be less controlled. The photo-assisted reduction method involves reducing metal ions using a reducing agent and a light source [7, 8]. In this method, a photosensitizer is added to the reaction mixture, which absorbs light and generates electron-hole pairs. These electrons then reduce the metal ions to form nanoparticles. The reducing agent provides additional electrons to the metal ions to facilitate their reduction. The

photo-assisted reduction method for producing nanoparticles offers several advantages, particle including controlled size, environmentally friendly (green) synthesis without toxic chemicals, high yield, and versatility for synthesizing different types of nanoparticles. These benefits are due to the ability to control particle size by adjusting light intensity and duration, making it a fast and efficient method with a high yield. Moreover, the method can be easily modified to produce nanoparticles with specific properties, making it a versatile approach to nanoparticle synthesis.

To ensure the production of high-quality and uniform silver nanoparticles (AgNPs), it is crucial to monitor their synthesis. Various methods can be employed for this purpose, including UVvisible spectroscopy, dynamic light scattering (DLS), transmission electron microscopy (TEM), X-ray diffraction (XRD), and Fourier transform (FTIR) spectroscopy. UV-visible spectroscopy is a simple and fast method but lacks information on nanoparticle size, shape, and distribution [9]. DLS can provide this information but requires expensive equipment [10]. TEM detailed characterization allows for nanoparticle size, shape, and morphology but is time-consuming and requires specialized equipment and expertise [11]. XRD provides insights into the crystal structure of nanoparticles but necessitates costly equipment and may not offer information on size and distribution. FTIR spectroscopy can provide information on surface functionalization and stability but requires specialized equipment and expertise [12]. While these methods offer valuable information on nanoparticle characteristics, they all involve postsynthesis measurements and cannot monitor the real-time generation rate or duration of nanoparticles during synthesis. Therefore, the development of a simple and cost-effective sensing platform to monitor the nanoparticle synthesis process is of great importance, as it would enable optimization of the production process by adjusting parameters such as reactant concentration, light intensity, and reaction temperature.

The LMR sensor is an optical sensor that uses the phenomenon of LMR to detect changes in the refractive index (RI) of a sample. The LMR effect was first reported by Marciniak, M. et al. in 1993 [13], when they demonstrated the effect in

optical dielectric waveguide with semiconductor thin-film cladding. Since then, LMR has been extensively studied, and various types of LMR sensors have been developed [14-17]. Another well-known phenomenon is surface plasmon resonance (SPR) [18-20], which occurs when the real part of the thin-film permittivity is negative and higher in magnitude than both its own imaginary part and the real part of the permittivity of the material surrounding the thin film (i.e., the optical waveguide and the surrounding medium in contact with the thin film). Compared to SPRs, LMRs offer some interesting properties, such as excitation under both TE and TM polarizations, the ability to generate several resonances in the same spectrum, and the easy control of the position of the resonance in the optical spectrum by increasing the thin-film thickness [21]. LMR sensors can be designed to operate in reflection or transmission mode, depending on the application requirements. They can be used for label-free detection of analytes in real-time [22-24], and can detect changes in RI with high sensitivity [25, 26], making them useful for a wide range of sensing applications [15, 16, 27, 281.

The optical planar waveguide-based LMR (OPWLMR) sensor is a type of optical sensor consisting of a metal-oxide thin-film on a lowloss dielectric waveguide. Compared to fiberbased sensors, the OPWLMR sensor offers several advantages, including a broader sensing range, a larger sensing zoom, and a simpler design that allows for easy integration with other optical components. Furthermore, OPWLMR sensors can be fabricated using low-cost, highvolume manufacturing processes, making them suitable for a wide range of applications, such as biomedical sensing, environmental monitoring, and food safety analysis [29, 30]. Overall, the LMR sensors have undergone significant developments and improvements over the past few decades, and they continue to attract research interest and hold enormous potential for various sensing applications.

In this study, we demonstrated a sensing platform that utilizes an OPWLMR sensor and combined with two blue LED arrays as the light source for irradiation. AgNPs were generated using the photo-assisted reduction method and deposited on the sensor. The illumination and duration of the blue light were controlled by

adjusting the LED driving voltage, and the resulting LMR wavelength shift caused by AgNPs deposition was measured to monitor the nanoparticle generation process in real-time. Finally, the size and distribution of AgNPs were measured using DLS.

II. METHODS

In the synthesis of AgNPs, a photoassisted reduction method was employed, utilizing blue LED light to facilitate the synthesis process. The energy from the blue light assisted in the formation of AgNPs, which were subsequently deposited onto the OPWLMR sensor. Due to LMR's high sensitivity to trace amounts of analytes, the formation of AgNPs shifts in the LMR signal's wavelength, allowing for real-time monitoring of their production. In this provide section, we comprehensive explanations of the two main methods utilized in the study.

2.1 Photo-assisted reduction

Photo-assisted reduction is an innovative approach for synthesizing AgNPs [7, 8, 31]. Unlike photo-mediated synthesis [32, 33], the key distinction lies in the absence of a pre-synthesized strong reducing agent for nano-crystal formation. Instead, this method relies on the generation of seed crystals with the assistance of light. In this study, silver nitrate was combined with a reducing agent (sodium borohydride) to facilitate the reduction of silver ions into metallic silver. The primary chemical formula (1) representing the reaction is provided below.

$$2AgNO_3 + 2N_aBH_4 \rightarrow H_2 + B_2H_6 + 2N_aNO_3 + 2Ag$$
 (1)

To obtain nanoscale crystals, a covering agent (sodium citrate) was introduced to prevent the aggregation of silver crystals and preserve their nanoscale properties. The reaction involved three chemicals: (1) silver nitrate as the source of silver ions, (2) sodium borohydride as the reducing agent, and (3) sodium citrate as the covering agent, stabilizer, and light-reducing agent necessary for the photo-reduction process. Unlike the conventional method that requires presynthesis of seed crystals, the photo-assisted reduction method circumvents issues associated with the intricate manipulation steps and

techniques involved in seed crystal synthesis. This eliminates variations in particle size distribution and inconsistencies in seed crystal morphology, thereby enhancing experimental reproducibility and convenience.

2.2 LMR operating principle

The operational principle of an LMR sensor is based on the resonant coupling phenomenon between a guided mode and a lossy mode within an optical waveguide structure [34, 35]. In an LMR sensor, a thin layer of high-refractive-index metal oxide is deposited on a low-refractiveindex optical fiber or waveguide. When light is coupled into the waveguide, it interacts with the thin layer, leading to the establishment of a resonance condition that manifests as a distinct dip in the transmission spectrum. From a materials and optics perspective, the propagation of light through an optical waveguide and its interaction with the metal oxide clad-waveguide interface induce changes in the charge carrier mobility within the metal oxide layer. These changes in mobility subsequently impact the conductivity of the lossy material, which directly correlates with its permittivity (ε_m). Consequently, any alteration in the conductivity of the lossy material triggers a variation in its permittivity, and the relative refractive index (n_m) can be expressed as eq.(2).

$$\varepsilon_{\rm m} = (n_{\rm m})^2 = (n + ik)^2$$
 (2)

As a result, any change in the permittivity induces modifications in both the real (n) and imaginary (k) components of the refractive index (RI). It is important to emphasize that the RI of dielectric materials exhibits wavelength dependency. In optical systems, as modes propagate through the core of an optical waveguide with metal oxide cladding, they become lossy within the cladding region. This rearrangement of modes gives rise to a resonance condition, which is influenced by the optical properties, including the RI of the metal oxide and the surrounding medium. The appearance of LMR is determined by the requirement that the real part of the overlay permittivity must be positive and possess a greater magnitude than both its own imaginary part and the real part of the permittivity of the materials adjacent to the overlay, such as the optical waveguide and the external medium.

The resonance wavelength of the LMR sensor

exhibits high sensitivity to variations in the RI of the surrounding material. When there are changes in the RI of the surrounding medium, such as in the presence of chemical or biological analytes [14, 22], the resonance wavelength undergoes a shift, leading to alterations in the optical transmission spectrum. This wavelength shift in LMR can be leveraged to detect and quantify the presence of analytes.

III. MATERIALS AND EXPERIMENTS

3.1 Materials and OPWLMR sensor fabrication

The AgNPs were synthesized using a photoassisted reduction method, employing blue LED light as the irradiation source. Silver nitrate, sodium borohydride, and sodium citrate were obtained from Sigma-Aldrich and used without further purification. Milli-Q grade water (>18.2 M Ω -cm) was utilized in all experiments. In a typical synthesis, 5 mL of sodium citrate (2.0× 10^{-3} M), 5 mL of sodium borohydride (2.0× 10^{-3} M) and 1 mL of silver nitrate (1.0 × 10^{-2} M) were mixed.

To assess the resonance effect and sensitivity of the OPWLMR sensor, solutions of glycerol in water with varying concentrations were prepared as test samples, and their respective RI were measured. Glycerol purchased from Huaho Chemical Co. in Taoyuan, Taiwan, was used as the analyte for evaluating the LMR sensor's performance. The analyte solution was prepared by dissolving glycerol in water and stirring the mixture for 10 minutes at room temperature using an electromagnetic stirrer. The RI of each glycerol solution was measured using a handheld refractometer (R5000, ATOAGO Co. Ltd.), with a minimum measurement scale of 0.001 RIU (RI unit). The corresponding RI values for glycerol in water solutions with concentrations ranging from 0% to 100% in 10% increments are presented in Table 1.

In the experiment, square soda-lime glass sheets obtained from Lifeco Optical Inc. in Taichung, Taiwan, with a thickness of 0.4 mm and a side length of 100 mm were used. These glass sheets underwent pre-cleaning procedures using acetone and purity wipes. The deposition of an indium tin oxide (ITO) thin film on the glass

sheets was carried out through sputtering, following methods described in our previous work [36]. After the sputtering process, the ITO-coated glass sheets were cut into 30 mm squares, which served as the OPWLMR sensor. The thickness of the ITO film was measured using an optical interferometer and found to be approximately 100 nm.

Table 1 RI for glycerol concentrations in water

Conc. %	0	10	20	30	40
RI	1.334	1.344	1.354	1.368	1.381
Conc. %	50	60	70	80	100

3.2 Experimental setup

The experimental setup included a halogen white light source (AQ4303B, Ando Electric Co. Ltd.), an optical spectrum analyzer (OSA, AQ6315A Ando Electric Co. Ltd.), and an OPWLMR sensor. Figure 1 provides a schematic diagram illustrating the details of experimental setup, along with a photograph showcasing the OPWLMR sensor held in place by the alignment bulk platform. The bulk platform was pre-designed to facilitate selfalignment, ensuring that the LMR sensor fit perfectly, with the optical axis aligned along the center of the sensor. An optical fiber patchcord with an FC connector connected the light source to the hole on the left-hand side of the platform, while another optical fiber patchcord was inserted into the right-hand side, connecting to the OSA.

The blue light source was assembled using 36 blue LEDs and 12 current-limiting resistors with a resistance of 390 ohms. These components were soldered onto a printed circuit board to create a single-sided $6x\hat{6}$ LED array. To enhance the light intensity, an additional LED array was positioned above and below the OPWLMR sensing platform, resulting in a total of 72 LEDs that could be simultaneously illuminated. The central wavelength of the blue LEDs was 460 nm, with a 3 dB line width of approximately 20 nm. The LED arrays were powered by a power supply unit, enabling the illumination to be adjusted by modifying the input voltage. To establish the relationship between the driving voltage and illuminance for one LED array, a photometer (Solar power meter TM-207, TENMARS Electronics Co. Ltd.) was employed. The photometer was placed at a distance of approximately 50 mm from the light source, and the measured results are depicted in Fig. 2.

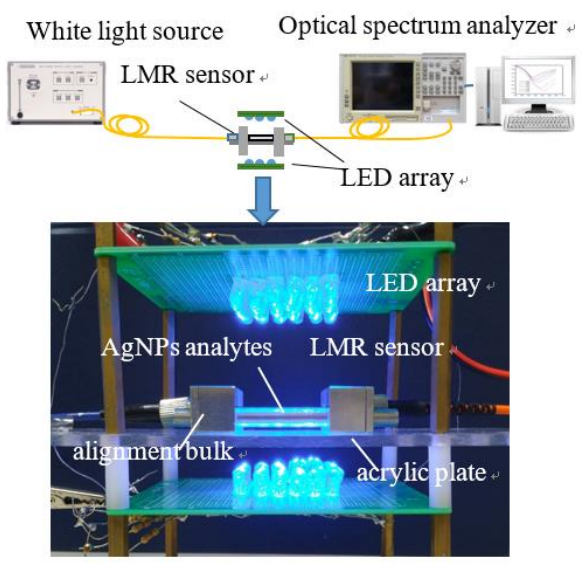


Fig. 1. The OPWLMR sensing platform.

The OPWLMR sensing platform was supported by a transparent acrylic plate (100×200×5 in mm), as shown in Fig. 1. Two LED array light sources were positioned 5 cm above and below the platform, respectively, to provide auxiliary light during the generation process of AgNPs. Subsequently, the prepared mixture for AgNPs was illuminated with the light source on the OPWLMR sensor.

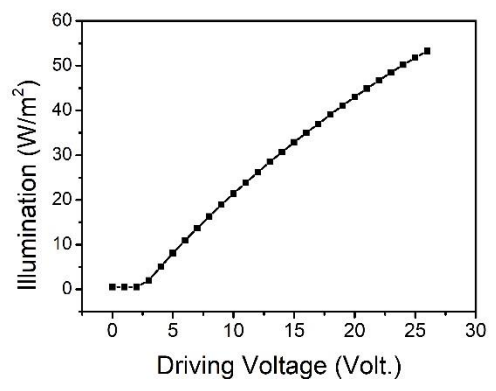


Fig. 2. The driving voltage and illuminance for one LED array.

IV. RESULTS AND DISCUSSIONS

4.1 OPWLMR sensor performance

The OPWLMR sensor functions based on the principle that even a slight change in the RI of the analyte leads to a wavelength shift in the LMR. Figure 3 illustrates the LMR spectrogram, where the x-axis represents the incident light wavelength, and the y-axis represents the transmission. The transmission is quantified as $T = P_1/P_0$, where P_0 represents the transmitted spectrum without the analyte, and P_1 represents the transmitted spectrum with the analyte. This normalization allows for a wavelength-dependent response to changes in external RI, relative to the spectrum of a bare sensor surrounded by air (P_0) .

For the measurement of external RI, the OPWLMR sensor was immersed in aqueous solutions of glycerol with varying RIs. The LMR wavelength corresponds to the point on the spectrum where the curve exhibits a dip, indicating maximum loss at a specific incident wavelength. The transmission spectrum was measured 30 times for each analyte with a different RI, and the average was calculated to obtain the spectral response. Figure 3 presents the spectral response for RIs ranging from 1.334 to 1.470. For an analyte with an RI of 1.334, the LMR wavelength is 880.5 nm. As the RI of the analyte increases, the LMR wavelength also increases to 961.4 nm, while the transmission decreases from 0.824 to 0.580. This indicates that analytes with higher RIs exhibit a more pronounced LMR effect.

The sensitivity of the OPWLMR sensor, which is defined as the ratio of the change in LMR wavelength to the change in analyte RI, is used to evaluate its performance. Since the LMR wavelength is highly sensitive to the RI of the analyte, a polynomial curve fitting is applied to obtain the equation (λ_{LMR}) as a function of the RI. The fitting curve is depicted in Fig.4, demonstrating a high goodness of fit with an R-square value of 0.995.

$$\lambda_{LMR}(n) = 6535.4 - 8594.1n + 3266.3n^2$$
 (3)

Then, taking the derivative of the above equation yields the sensitivity (S) as eq. (4).

$$S = \frac{d\lambda_{LMR}}{dn} = -8594.1 + 6532.6n \tag{4}$$

According to the estimation provided in eq. (4), the sensitivity of the OPWLMR sensor gradually increases from 120.4 nm/RIU to 1008.9 nm/RIU as the RI of the analyte increases. These results are consistent with the findings reported in reference [37]. It is worth noting that the reported sensitivities for LMR sensors vary depending on the specific parameters, such as the thickness of the ITO layer. For instance, previous studies have reported sensitivities of 2953 nm/RIU and 1617

nm/RIU for ITO layers with thicknesses of 115 nm and 220 nm, respectively [37]. Table 2 provides a comparison of the sensitivity of different LMR sensors. Although the OPWLMR sensor in this study may have slightly lower sensitivity compared to some optical fiber LMR sensors, it offers several advantages. The OPWLMR sensor features a simple and robust structure that utilizes cost-effective materials, enabling easy mass production. Additionally, the sensor is highly compatible with surface modification techniques, making it well-suited for various bio-sensing applications.

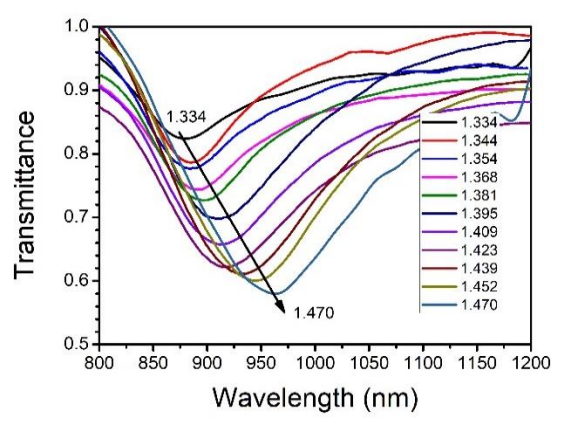


Fig. 3. Spectral response for RIs ranging from 1.334 to

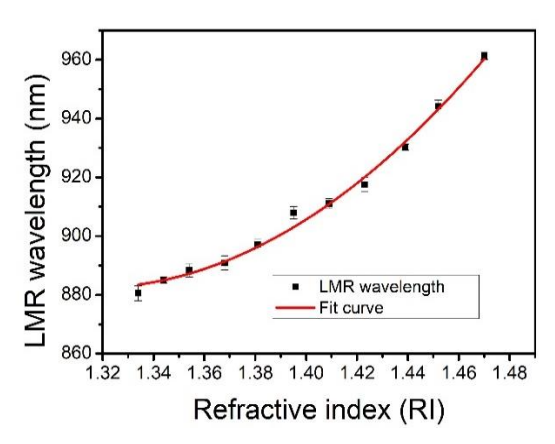


Fig. 4. The LMR wavelength as a function of RIs and the fitting curve.

Table 2 Comparison of sensitivity of LMR Sensors

material	configuration	Sensitivity	Ref.
ITO	MMF	2953 nm/RIU	[37]
ITO	D-shaped	8742 nm/RIU	[38]
ZnO	U-shaped	220 nm/RIU	[39]
AZO	MMF	1154 nm/RIU	[40]
ITO	OPW	1009 nm/RIU	this work

4.2 AgNPs detection with LMR

In this experiment, the pre-mixed solution of reactants was dropped onto an OPWLMR sensing platform with the blue LED light source, and the LMR sensing spectrum was recorded. The initial LMR wavelength was measured 5 minutes after dropping of the reactants, and subsequent LMR wavelength shifts were recorded every 5 minutes for a total duration of 60 minutes. This investigation aimed to explore the relationship between the generation of AgNPs and the duration of illumination. Additionally, the effect of light intensity on the generation of AgNPs was examined by adjusting the driving voltage of the light source. Fig. 5 illustrates the results obtained when the driving voltage was gradually increased from 11 V to 23 V. It was observed that a minimum voltage of 19 V was required to provide sufficient light intensity for assisting in the generation of AgNPs. It is noteworthy that the duration required for AgNPs generation and deposition on the sensing platform varied depending on the resonance wavelength and eventually reached a steady state. Moreover, the duration of AgNPs generation and deposition on the sensing platform was found to be influenced by the intensity of light irradiation and tended to reach a steady state. Specifically, stronger light irradiation at 23 V resulted in a shorter required time of approximately 15 minutes, whereas weaker light irradiation at 19 V necessitated a longer time of approximately 20 minutes.

4.3 AgNPs specification

In the experiment, the DLS instrument (ELSZ-2000, Otsuka Tech Electronics Co., Ltd., Japan) was operated under the following conditions: temperature of 25 °C, detector angle of 165 degrees, incident laser wavelength of 660 nm, and laser power of 70 mW. The generated AgNPs sample was first diluted by adding 0.5 ml of the sample to 2 ml of deionized (DI) water, followed by sonication at 40 kHz for 30 seconds. Possible interfering impurities were removed by passing the sample through a 0.45 μ m filter, and the resulting solution was subsequently analyzed using DLS.

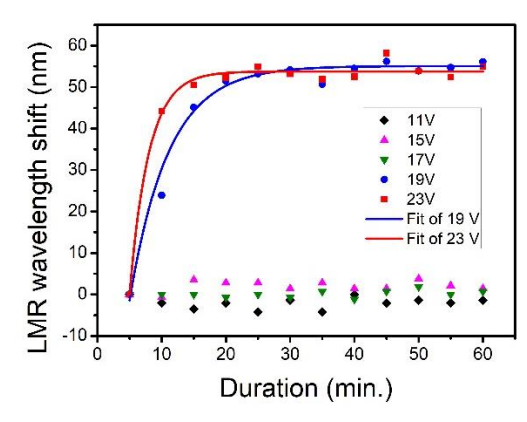


Fig. 5. The LMR wavelength shift during AgNPs generation for LED array driving voltage increased from 11 V to 23 V.

The particle size distribution of AgNPs exhibited two distinct groups, as illustrated in Fig. 6. The first group consisted of smaller particles ranging from 1 nm to 4 nm, with a lower particle count and an average size of 2.2 nm. The second group comprised larger particles ranging from 16 nm to 86 nm, with a higher particle count and an average size of 41.8 nm. The overall average cumulant diameter was determined to be 21.3 nm. The smaller size group is believed to be coated with a capping agent, preventing further accumulation of silver atoms. No AgNPs with a diameter larger than 98 nm were detected in the sample. The cumulant intensity for D10, D50, and D90 are provided in Table 3, indicating that 90% of the particles have sizes smaller than 56.5 nm.

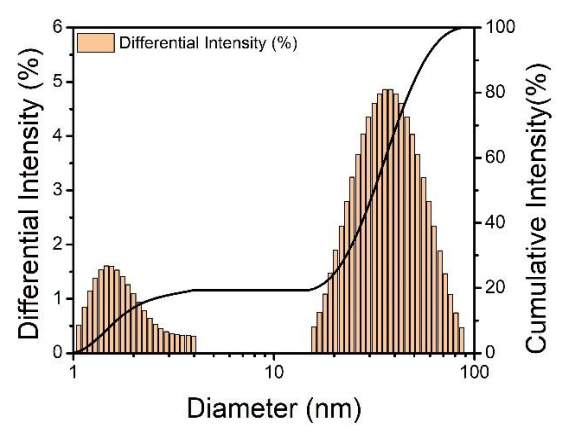


Fig. 6 The particle size distribution of AgNPs.

Table 3 The cumulant diameter list for AgNPs

Cum. Dia. (nm)	D10	D50	D90
21.3	1.6	31.6	56.5

IV. CONCLUSIONS

In this article, we propose a novel method, to the best of our knowledge, for real-time monitoring of the synthesis process of AgNPs. This method employs a simple and cost-effective setup consisting of an OPWLMR sensor combined with two blue LED arrays. The AgNPs synthesized using a photo-assisted reduction method and subsequently deposited on the sensor surface. Our findings indicate that a minimum driving voltage of approximately 19 V (corresponding to an illumination of 41.1 W/m²) is required to facilitate the generation of AgNPs, and the deposition process typically takes between 15 to 20 minutes. These results demonstrate the feasibility of using our proposed sensing platform to monitor the relationship between the generation process and the required deposition duration of AgNPs. Moreover, this approach has the potential to optimize nanoparticle synthesis processes and offers promising prospects for the development of various nanoparticle types in future applications.

REFERENCES

- [1] A. Naganthran *et al.*, "Synthesis, characterization and biomedical application of silver nanoparticles," *Materials*, vol. 15, no. 2, p. 427, 2022.
- [2] V. Eskandari *et al.*, "Coating of silver nanoparticles (AgNPs) on glass fibers by a chemical method as plasmonic surface-enhanced Raman spectroscopy (SERS) sensors to detect molecular vibrations of Doxorubicin (DOX) drug in blood plasma," *Arabian Journal of Chemistry*, vol. 15, no. 8, p. 104005, 2022.
- [3] P. Zhan *et al.*, "A fibrous flexible strain sensor with Ag nanoparticles and carbon nanotubes for synergetic high sensitivity and large response range," *Composites Part A: Applied Science and Manufacturing*, p. 107431, 2023.
- [4] Y. Liu, F. Wang, L. Li, F. Cao, B. Zhu, and Y. Gu, "Linear and nonlinear optical properties of AgNPs and AgNPs/graphene composites modulated by localized surface plasmon resonance effect," *JOSA B*, vol. 39, no. 3, pp. 713-721, 2022.
- [5] R. Shanmuganathan *et al.*, "Synthesis of silver nanoparticles and their biomedical

- applications-a comprehensive review," *Current pharmaceutical design,* vol. 25, no. 24, pp. 2650-2660, 2019.
- [6] C. Quintero-Quiroz *et al.*, "Optimization of silver nanoparticle synthesis by chemical reduction and evaluation of its antimicrobial and toxic activity," *Biomaterials research*, vol. 23, no. 1, pp. 1-15, 2019.
- [7] L.-C. Yang, Y.-S. Lai, C.-M. Tsai, Y.-T. Kong, C.-I. Lee, and C.-L. Huang, "One-pot synthesis of monodispersed silver nanodecahedra with optimal SERS activities using seedless photo-assisted citrate reduction method," *The Journal of Physical Chemistry C*, vol. 116, no. 45, pp. 24292-24300, 2012.
- [8] J. A. Badmus *et al.*, "Photo-assisted biofabrication of silver nanoparticles using Annona muricata leaf extract: exploring the antioxidant, anti-diabetic, antimicrobial, and cytotoxic activities," *Heliyon*, vol. 6, no. 11, p. e05413, 2020.
- [9] W. M. Shume, H. A. Murthy, and E. A. Zereffa, "A review on synthesis and characterization of Ag2O nanoparticles for photocatalytic applications," *Journal of Chemistry*, vol. 2020, pp. 1-15, 2020.
- [10] F. E. a. Meva *et al.*, "Silver and palladium nanoparticles produced using a plant extract as reducing agent, stabilized with an ionic liquid: sizing by X-ray powder diffraction and dynamic light scattering," *Journal of Materials Research and Technology*, vol. 8, no. 2, pp. 1991-2000, 2019.
- [11] N. Ortiz Peña *et al.*, "Morphological and structural evolution of Co3O4 nanoparticles revealed by in situ electrochemical transmission electron microscopy during electrocatalytic water oxidation," *ACS nano*, vol. 13, no. 10, pp. 11372-11381, 2019.
- [12] N. Ortega-Hernández, M. Ortega-Romero, M. Medeiros-Domingo, O. C. Barbier, and M. Rojas-López, "Detection of Biomarkers Associated with Acute Kidney Injury by a Gold Nanoparticle Based Colloidal Nano-Immunosensor by Fourier-Transform Infrared Spectroscopy with Principal Component Analysis," *Analytical Letters*, vol. 55, no. 15, pp. 2370-2381, 2022.
- [13] M. Marciniak, J. Grzegorzewski, and M. Szustakowski, "Analysis of lossy mode cutoff conditions in planar waveguides with semiconductor guiding layer," *IEE Proceedings J-Optoelectronics*, vol. 140, no. 4, pp. 247-252, 1993.

- [14]P. Zubiate, C. R. Zamarreño, P. Sánchez, I. R. Matias, and F. J. Arregui, "High sensitive and selective C-reactive protein detection by means of lossy mode resonance based optical fiber devices," *Biosensors and Bioelectronics*, vol. 93, no. Supplement C, pp. 176-181, 2017/07/15/2017.
- [15] X. Wang, Q. Wang, Z. Song, and K. Qi, "Simulation of a microstructure fiber pressure sensor based on lossy mode resonance," *AIP Advances*, vol. 9, no. 9, p. 095005, 2019.
- [16] X.-P. Jin *et al.*, "High-sensitivity fiber optic magnetic field sensor based on lossy mode resonance and hollow core-offset structure," *Instrumentation Science & Technology*, pp. 1-12, 2021.
- [17] P. I. Kuznetsov, D. P. Sudas, and E. A. Savelyev, "Fiber optic Lossy Mode Resonance based sensor for aggressive liquids," *Sensors and Actuators A: Physical*, vol. 321, p. 112576, 2021/04/15/2021.
- [18] J. Homola and M. Piliarik, "Surface Plasmon Resonance (SPR) Sensors," in *Surface Plasmon Resonance Based Sensors*, J. Homola, Ed. Berlin, Heidelberg: Springer Berlin Heidelberg, 2006, pp. 45-67.
- [19] P. J. Rivero, A. Urrutia, J. Goicoechea, and F. J. Arregui, "Optical fiber humidity sensors based on Localized Surface Plasmon Resonance (LSPR) and Lossy-mode resonance (LMR) in overlays loaded with silver nanoparticles," *Sensors and Actuators B: Chemical*, vol. 173, pp. 244-249, 10// 2012
- [20] A. E. Lidiya, R. V. J. Raja, Q. M. Ngo, and D. Vigneswaran, "Detecting hemoglobin content blood glucose using surface plasmon resonance in D-shaped photonic crystal fiber," *Optical Fiber Technology*, vol. 50, pp. 132-138, 2019.
- [21] I. Del Villar *et al.*, "Design rules for lossy mode resonance based sensors," *Applied optics*, vol. 51, no. 19, pp. 4298-4307, 2012.
- [22] B. Li, R. Zhang, R. Bi, and M. Olivo, "Applications of Optical Fiber in Label-Free Biosensors and Bioimaging: A Review," *Biosensors*, vol. 13, no. 1, p. 64, 2023.
- [23] M. Śmietana *et al.*, "Simultaneous optical and electrochemical label-free biosensing with ITO-coated lossy-mode resonance sensor," *Biosensors and Bioelectronics*, vol. 154, p. 112050, 2020/04/15/ 2020.
- [24] C. R. Zamarreño *et al.*, "Route Towards a Label-free Optical Waveguide Sensing

- Platform Based on Lossy Mode Resonances," *Sensors & Transducers Journal*, vol. 11, no. 138, 2019.
- [25] G. S. Mei, P. S. Menon, and G. Hegde, "ZnO for performance enhancement of surface plasmon resonance biosensor: a review," *Materials Research Express*, vol. 7, no. 1, p. 012003, 2020.
- [26] R. Verma, "Sensitivity enhancement of a lossy mode resonance based tapered fiber optic sensor with an optimum taper profile," *Journal of Physics D: Applied Physics*, vol. 51, no. 41, p. 415302, 2018.
- [27] D. Bohorquez, I. Del Villar, J. Corres, and I. Matias, "Wavelength and intensity based lossy mode resonance breathing sensor," *Optics & Laser Technology*, vol. 140, p. 107063, 2021.
- [28] D. Tiwari, K. Mullaney, S. Korposh, S. W. James, S.-W. Lee, and R. P. Tatam, "An ammonia sensor based on Lossy Mode Resonances on a tapered optical fibre coated with porphyrin-incorporated titanium dioxide," *Sensors and Actuators B: Chemical*, vol. 242, pp. 645-652, 4// 2017.
- [29] O. Fuentes, J. Goicoechea, J. M. Corres, I. Del Villar, A. Ozcariz, and I. R. Matias, "Generation of lossy mode resonances with different nanocoatings deposited on coverslips," *Optics Express*, vol. 28, no. 1, pp. 288-301, 2020.
- [30] I. R. Matias, I. Del Villar, and J. M. Corres, "Lossy mode resonance based sensors in planar configuration: a review," *IEEE Sensors Journal*, 2023.
- [31] L. A. Ningsih *et al.*, "Ag-modified TiO2/SiO2/Fe3O4 sphere with core-shell structure for photo-assisted reduction of 4-nitrophenol," *Environmental Research*, vol. 214, p. 113690, 2022.
- [32] J. K. Patra, G. Das, A. Kumar, A. Ansari, H. Kim, and H.-S. Shin, "Photo-mediated biosynthesis of silver nanoparticles using the non-edible accrescent fruiting calyx of Physalis peruviana L. fruits investigation of its radical scavenging and cytotoxicity potential activities," ofJournal *Photochemistry* Photobiology B: Biology, vol. 188, pp. 116-125, 2018.
- [33] G. Das, H.-S. Shin, A. Kumar, C. N. Vishnuprasad, and J. K. Patra, "Photomediated optimized synthesis of silver nanoparticles using the extracts of outer shell fibre of Cocos nucifera L. fruit and

- detection of its antioxidant, cytotoxicity and antibacterial potential," *Saudi Journal of Biological Sciences*, vol. 28, no. 1, pp. 980-987, 2021.
- [34] Q. Wang and W.-M. Zhao, "A comprehensive review of lossy mode resonance-based fiber optic sensors," *Optics and Lasers in Engineering*, vol. 100, pp. 47-60, 1// 2018.
- [35] I. Del Villar *et al.*, "Optical sensors based on lossy-mode resonances," *Sensors and Actuators B: Chemical*, vol. 240, pp. 174-185, 2017.
- [36] Y.-C. Lin and L.-Y. Chen, "Development of a Temperature-Controlled Optical Planar Waveguide Sensor with Lossy Mode Resonance for Refractive Index Measurement," in *Photonics*, 2021, vol. 8, no. 6: MDPI, p. 199.
- [37] I. D. Villar, C. R. Zamarreno, M. Hernaez, F. J. Arregui, and I. R. Matias, "Lossy Mode Resonance Generation With Indium-Tin-Oxide-Coated Optical Fibers for Sensing Applications," *Journal of Lightwave Technology*, vol. 28, no. 1, pp. 111-117, 2010.
- [38] P. Zubiate, C. Zamarreño, I. Del Villar, I. Matias, and F. Arregui, "High sensitive refractometers based on lossy mode resonances (LMRs) supported by ITO coated D-shaped optical fibers," *Optics express*, vol. 23, no. 6, pp. 8045-8050, 2015.
- [39] N. Paliwal, N. Punjabi, J. John, and S. Mukherji, "Design and Fabrication of Lossy Mode Resonance Based U-Shaped Fiber Optic Refractometer Utilizing Dual Sensing Phenomenon," *Journal of Lightwave Technology*, vol. 34, no. 17, pp. 4187-4194, 2016.
- [40] A. Ozcariz, D. A. Piña-Azamar, C. R. Zamarreño, R. Dominguez, and F. J. Arregui, "Aluminum doped zinc oxide (AZO) coated optical fiber LMR refractometers—An experimental demonstration," *Sensors and Actuators B: Chemical*, vol. 281, pp. 698-704, 2019/02/15/2019.